Supporting Information

Morphological Characteristics, Hemoglobin Content, and Membrane Mechanical Properties of Red Blood Cell Delivery Systems

Thompson Lu,[†] Chi-Hua Lee, [‡] and Bahman Anvari[†,‡*]

[†] Department of Bioengineering, University of California, Riverside, Riverside, CA 92521, USA

[‡] Department of Biochemistry, University of California, Riverside, Riverside, CA 92521, USA

* E-mail: anvarib@ucr.edu

Illustrative Calibration Results. We present illustrative calibration results for the position sensitive detector (PSD) output voltage against the displacement of the trapped bead (Figure S1), and the applied drag force against the PSD output voltage (Figure S2).

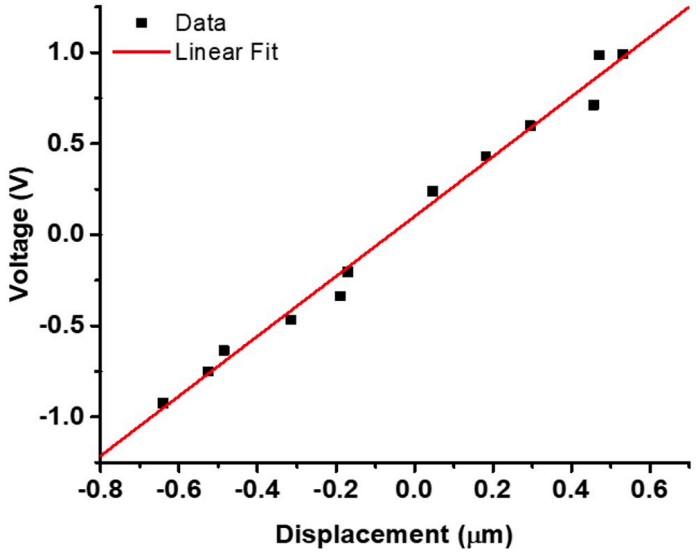

Figure S1. Displacement calibration. Measured PSD output voltage for various displacements of the trapped bead, and the linear fit to the experimental results are shown. The equation of the linear fit is: Voltage = 1.643 (displacement) – 0.101.

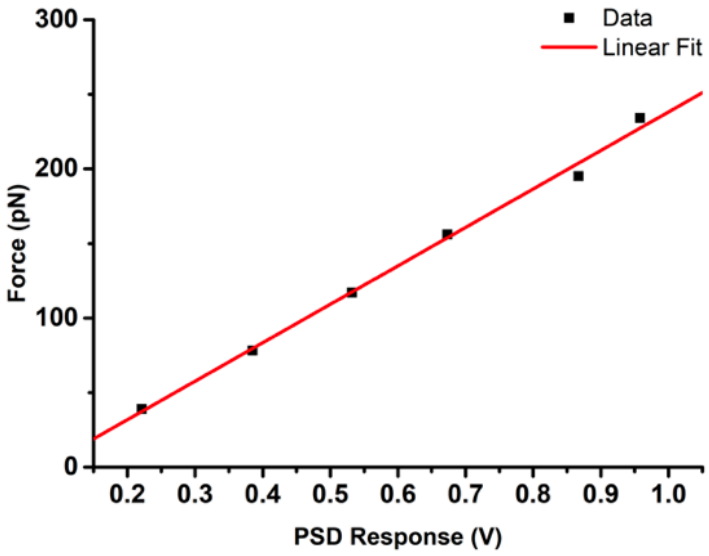

Figure S2. Force calibration. Experimentally obtained values of the drag force on trapped beads as a function of PSD output voltage, and the linear fit are shown. Equation of the linear fit is: Force = 257.8 (Voltage) + 19.7

Phase Maps of Polystyrene beads, RBC Ghosts, and RBC Ghosts$_{ICG}$. As part of our methodology to estimate the refractive index of blood plasma, and the membrane of RBC Ghosts, we used QPI to obtain the relevant phase maps of the beads (Figure S3), and those of RBC Ghosts and RBC Ghosts$_{ICG}$ and (Figure S4).

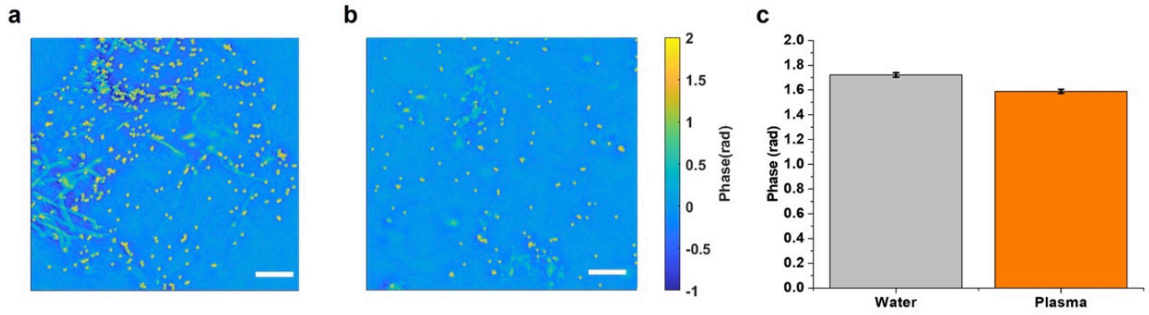

Figure S3. QPI-based imaging of polystyrene beads. (a) Phase map of 630 µm diameter beads in water. (b) Phase map of 630 nm diameter beads in in blood plasma. Scale bars represent 10 µm on panels a and b. (c) Average phase values of the beads in water and plasma. Error bars represent SEs (Number of samples in plasma = 48, Number of samples in plasma = 72).

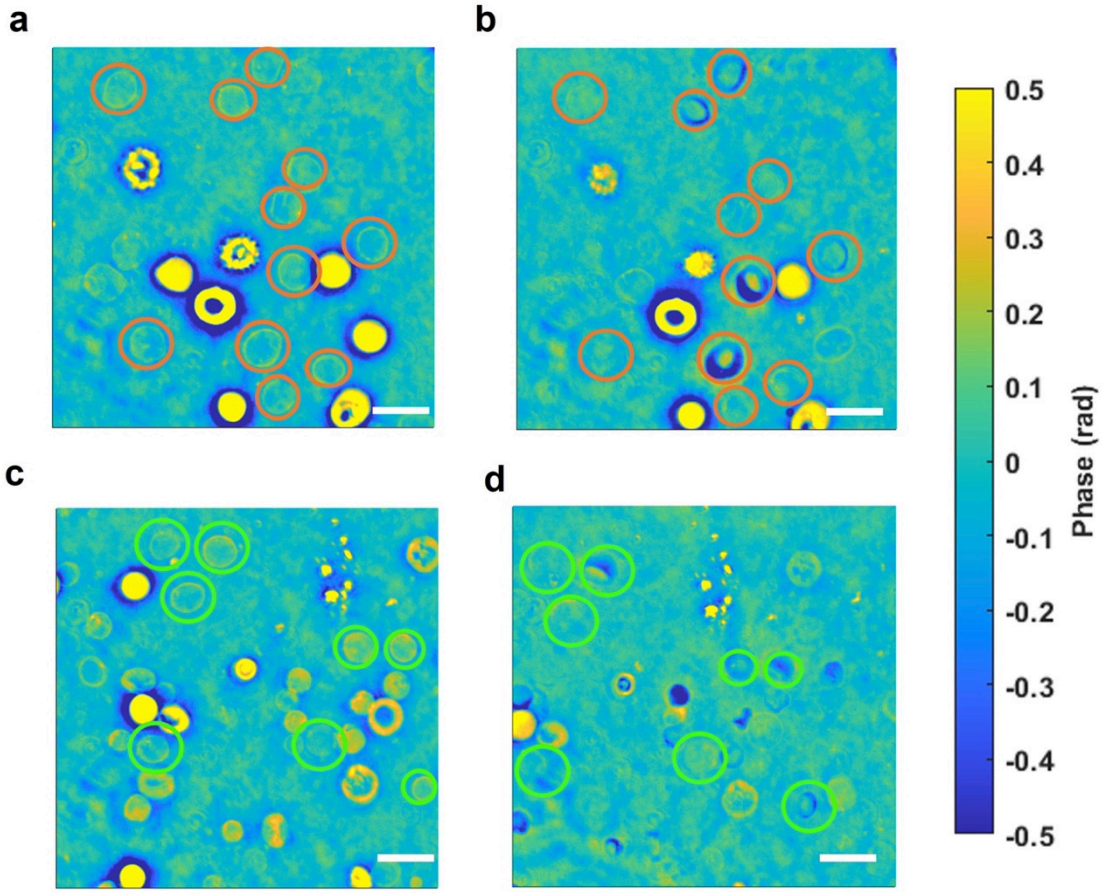

Figure S4. QPI-based imaging of RBC Ghosts and RBC $Ghosts_{ICG}$. (a) Phase map of RBC Ghosts in 1X PBS. (b) Phase map of RBC Ghosts in blood plasma. (c) Phase map of RBC $Ghosts_{ICG}$ in 1X PBS. (d) Phase map of RBC $Ghosts_{ICG}$ in blood plasma. Scale bars represent 10 μm on panels a-d. Illustrative RBC Ghosts are shown by orange circles in panels a, and b. Illustrative RBC $Ghosts_{ICG}$ are shown by green circles in panels c, and d.

Mechanical Model. We used a five-parameter generalized Maxwell-Weichert model (Figure S5) to fit the experimentally-measured force relaxation profiles associated with membrane tethers pulled from RBCs, RBC Ghosts, and RBC Ghosts$_{ICG}$, and estimate the viscoelastic properties of their membranes. In this model, three springs with stiffness values k_1, k_2, k_3 (pN/μm), and two dashpots with friction coefficients μ_1 and μ_2 (pN•s/μm) are used to model the elastic and viscous behavior of the membrane, respectively.

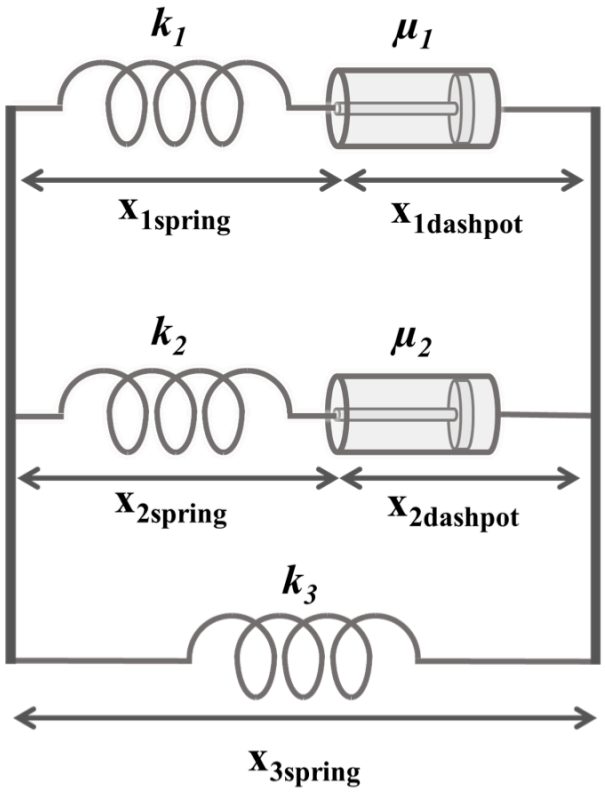

Figure S5. Five-parameter Generalized Maxwell-Weichert body. The model consists of thee springs and two dashpots, and was used to fit the experimentally-obtained tether force relaxation profiles to estimate the values of the mechanical parameters.

The governing equation for this mechanical model can be written as:

$$F + (\tau_1 + \tau_2)\frac{dF}{dt} + \tau_1\tau_2\frac{d^2F}{dt^2} =$$

$$k_3x + (k_0\tau_1 + \mu_1 + k_3\tau_2 + \mu_2)\frac{dx}{dt} + (k_0\tau_1\tau_2 + \mu_1\tau_2 + \mu_2\tau_1)\frac{d^2x}{dt^2} \quad \text{(S1)}$$

where x is the induced deformation, t is time, and τ are the corresponding characteristic relaxation times for each of the two spring-dashpot Maxwell bodies:

$$\tau_i = \frac{\mu_i}{k_i},\ i = 1,2 \quad \text{(S2)}$$

During an experiment, a membrane tether is elongated at a constant rate (V) of 1 μm/s until a specified length (L). When tether pulling stops, we assume there is an instantaneous change in the tether pulling velocity from 1 μm/s to zero. Since the tether force at this transition remains continuous, the elements that can instantaneously respond to this abrupt change in velocity are the springs. Therefore, the change in velocity is shared equally among the three springs:

$$\left.\frac{dx_{1_{spring}}}{dt}\right|_{t=t'} = \left.\frac{dx_{2_{spring}}}{dt}\right|_{t=t'} = \left.\frac{dx_{3_{spring}}}{dt}\right|_{t=t'} = -V \quad \text{(S3)}$$

where t' is the time at which tether pulling stops. The tether force reaches a steady state value (F_{ss}) at the end of elongation. The initial conditions at the start of the relaxation time are:

$$F(t = t') = F_{ss}, \quad \text{(S4)}$$

$$\left.\frac{dF}{dt}\right|_{t=t'} = \frac{dF_{ss}}{dt} - V(k_1 + k_2 + k_3). \quad \text{(S5)}$$

The solution to Equation S1 with the initial conditions given in Equations S4) and S5 is given as:

$$F(t) = F_{eq} + Ae^{-\left(\frac{t-t'}{\tau_1}\right)} + Be^{-\left(\frac{t-t'}{\tau_2}\right)}, \quad \text{(S6)}$$

where the coefficients A and B are:

$$A = \left(\frac{\tau_1}{\tau_1-\tau_2}\right)\left[F_{ss} - \tau_2\left(\frac{dF_{ss}}{dt} - V(k_1+k_2+k_3)\right) - F_{eq}\right], \quad \text{(S7)}$$

$$B = \left(\frac{\tau_2}{\tau_2-\tau_1}\right)\left[F_{ss} - \tau_1\left(\frac{dF_{ss}}{dt} - V(k_1+k_2+k_3)\right) - F_{eq}\right]. \quad \text{(S8)}$$

In Equations S7) and S8), F_{eq} is defined as the equilibrium force at the end of tether relaxation, and was determined by averaging the last 20 seconds of the tether force data. We then estimated the value of k_3 as:

$$k_3 = \frac{F_{eq}}{(L+dL)} \quad \text{(S9)}$$

where dL is the change in the tether length at the end of force relaxation.

Absorption Spectra. Illustrative absorption spectra for RBC Ghosts and RBC Ghosts$_{ICG}$ are presented in Fig. S1. The maxima at 415, 547 and 578 nm, respectively, correspond to the Soret peak, the fundamental (Q_0) and the vibronic tone (Q_V) of the Q-bands associated with porphyrin $\pi \rightarrow \pi^*$ transitions. The absorption peak at 802 nm for RBC Ghosts$_{ICG}$ is associated with the monomer form of ICG.

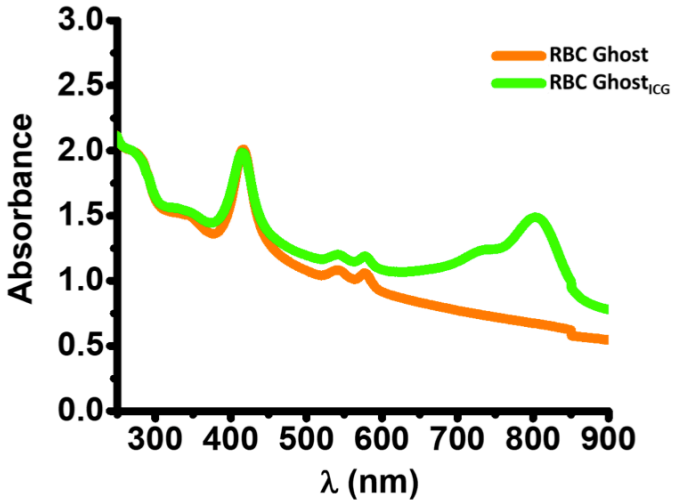

Figure S6. Absorption spectra of RBC Ghosts, and RBC Ghosts$_{ICG}$. For the spectral recordings, constructs were suspended in isotonic PBS (310 mOsm). RBC Ghosts$_{ICG}$ were fabricated using 100 μM ICG.

Video S1. Tether pulling from an RBC. An optically trapped 4.2 μm diameter lysine-coated polystyrene bead (on the left) was brought to the RBC. The bead and the RBC were allowed to adhere at t=1 second. The cell then was displaced away from the bead at a constant speed of 1 μm/s for 10 μm. Tether formation is indicated by the sudden displacement of the optically trapped bead at t=2 seconds. The tether was then allowed to relax to equilibrium. Note the dramatic change in morphology of the RBC from biconcave discoidal into a "bullet-like" shape. The tether pulling video was sped up by 18X.

Video S2. Tether pulling from an RBC Ghost. An optically trapped 4.2 μm diameter lysine-coated polystyrene bead (on the right) was brought to the RBC Ghost. The bead and the sample were allowed to adhere at t = 1 second. The RBC Ghost was then displaced away from the bead at a constant speed of 1 μm/s for 10 μm. Tether formation is indicated by the sudden displacement of the optically trapped bead at $t \sim 2.5$ seconds. The tether was then allowed to relax to equilibrium. Note that the spherical morphology of the RBC Ghost remains consistent throughout the tether pulling process, indicating low deformability. The tether pulling video was sped up by 18x.

Video S3. Tether pulling from an RBC $\text{Ghost}_{\text{ICG}}$. An optically trapped 4.2 μm diameter lysine-coated polystyrene bead (on the left) was brought to the RBC $\text{Ghost}_{\text{ICG}}$. The bead and the sample were allowed to adhere at t = 2 seconds. The RBC $\text{Ghost}_{\text{ICG}}$ was then displaced away from the bead at a constant speed of 1 μm/s for 10 μm. Tether formation is indicated by the sudden jump of the optically trapped bead at $t \sim 3.5$ seconds. The tether was then allowed to relax to equilibrium during the tether pulling process. The spherical morphology of the RBC $\text{Ghost}_{\text{ICG}}$ remains relatively consistent throughout the tether pulling process. The tether pulling video was sped up 18x.